Structural arrest in concentrated cytochrome C solutions: the effect of pH and salts

2004 J. Phys.: Condens. Matter 16 S5003

(http://iopscience.iop.org/0953-8984/16/42/016)

INSTITUTE OF PHYSICS PUBLISHING JOURNAL OF PHYSICS: CONDENSED MATTER

J. Phys.: Condens. Matter **16** (2004) S5003–S5022 PII: S0953-8984(04)79426-6

Structural arrest in concentrated cytochrome C solutions: the effect of pH and salts

P Baglioni[1,2,3], E Fratini[1], B Lonetti[1] and S H Chen[2,3]

[1] Department of Chemistry and CSGI, University of Florence, Sesto Fiorentino, 50019 Florence, Italy
[2] Department of Nuclear Engineering, Massachusetts Institute of Technology, Cambridge, MA 02139, USA

E-mail: baglioni@csgi.unifi.it and sowhsin@mit.edu

Received 13 April 2004, in final form 10 September 2004
Published 8 October 2004
Online at stacks.iop.org/JPhysCM/16/S5003
doi:10.1088/0953-8984/16/42/016

Abstract

The effect of pH and different anions of sodium salts on concentrated solutions of cytochrome C protein have been investigated by means of small angle neutron scattering and viscosity measurements. The control and a fine tuning of protein–protein interactions leads to the formation of protein clusters that eventually evolve into a structural arrested state. The appearance of a low Q peak in the small angle neutron scattering intensity distributions is also accompanied by a strong increase in the relative viscosity. These phenomena taken together can be considered as the signature of the gelation process. This structural arrest is induced by salt addition and specifically depends on the nature of anions, according to the Hofmeister series.

1. Introduction

Understanding the interaction between proteins in solution is crucial for physics, chemistry and biology for a number of reasons. The aggregation of proteins has a critical importance in a wide variety of situations ranging from pathologic states (human cataract, Alzheimer's and Parkinson's diseases) to the production, stability, and delivery of protein drugs, and to single crystal preparation in order to elucidate the three-dimensional structures of proteins themselves [1]. Moreover, proteins can be seen as model systems in colloidal science, as they have well-defined properties. The low charge, coupled with the relatively small sizes (10–50 Å) and mono-dispersity, render proteins an ideal model system to validate theories, such as the mode-coupling theory (MCT) [2], that try to explain metastable arrested states. Since the interactions between biopolymers in solution are mediated by water, co-solutes can influence both the surface of the macromolecule and the structure of the solvent (water). A milestone in

[3] Authors to whom any correspondence should be addressed.

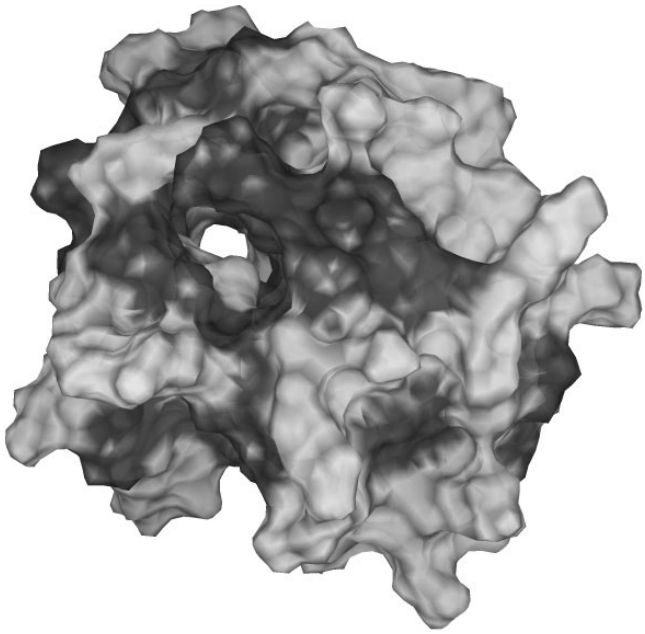

Figure 1. Horse heart cytochrome C (structure 1akk downloaded from the RCSB Protein Data Bank http://www.rcsb.org/pdb/). Hydrophobic residues are highlighted in dark grey while hydrophilic residues are in light grey. Although the molecule is globular, it is clearly not spherical. The heme group is not shown to clearly evidence the inside cavity where it is located.

the study of the effect of small molecules on proteins is represented by the work of Hofmeister. He investigated the efficiency of various salts in precipitating or salting-out ovalbumin, the main protein of egg white, from aqueous solutions. As a result, he found that the efficiency strongly depends on the kind of salt used at a fixed ionic strength [3]. For example for the anions, the efficiency follows the order: $SO_4^{2-} > F^- > Cl^- > Br^- > NO_3^- > I^- > ClO_4^- > SCN^-$. These results have been extended to many other proteins [4] and to their conformational stabilization [5]. The anion sequence is now accepted as the Hofmeister or lyotropic series (HS). The substances having a greater ability of salting-out, on the left-hand side of the series, are called kosmotropic substances (kosmotropes) whereas those having a weaker ability for the salting-out of proteins, on the right-hand side, are called chaotropic substances (chaotropes). Ducruix and co-workers demonstrated that the effectiveness of anions to promote protein crystallization is dependent on the net charge of the protein: for acidic proteins it follows HS (i.e. *Hypoderma lineatum* collagenase (isoelectric point, pI = 4.1) at pH 7.2 [6]), whereas the order is reversed for basic proteins (i.e. hen egg white lysozyme (pI = 11.0) at pH 4.5 [7]).

Horse heart cytochrome C is a small globular protein (see figure 1) consisting of 104 amino acids, 12 negatively charged (Glu, Asp) and 21 positively charged (Lys, Arg) and is characterized by a pI of about 10.2. Its molecular weight is 12 384 Da and its shape in aqueous solutions is approximately spherical ($a \times b \times b = 15 \times 17 \times 17$ Å^3). Cytochrome C is used in this study as a model for investigating the effect of pH and salt on the protein–protein interactions by means of both neutron scattering and rheological techniques. The pH and salt modulate the repulsive contribution in the interaction potential and the attractive part of the interaction potential becomes important around the pI of the protein. A specificity of the added anion is discussed in terms of the Hofmeister series [3].

Table 1. Cytochrome C sample composition at the two different investigated pD. The ionic strength, I^*, has been calculated considering only the NaOH contribution.

pD = 5.4 ± 0.1			pD = 11.0 ± 0.1		
ϕ	[c] (mM)	I^* (mM)	ϕ	[c] (mM)	I^* (mM)
0.100	9.15	—	0.093	8.48	45
0.201	18.35	—	0.198	18.10	95
0.300	27.41	—	0.299	27.33	142
0.400	36.59	—	0.400	36.56	192
0.500	45.72	—	0.496	45.39	238

2. Experimental section

2.1. Material

Cytochrome C from horse heart (product no C7752) was purchased from Sigma Chemical Company. This product is obtained using a procedure that avoids the trichloroacetic acid (TCA), which is known to promote the dimer formation in favour of the native protein.

In order to check how the pD affect the intermolecular interactions in cytochrome C solutions we prepared two sets of protein samples in D_2O at different pD, 5.4 and 11.0, with a protein volume fraction, ϕ, ranging from 0.1 to 0.5. SANS and rheological investigations were performed on the two sets prepared at the same time. A detailed list of the samples is reported in table 1. Acidic samples (pD = 5.4) were obtained by dissolving cytochrome C in D_2O, while the basic ones (pD = 11.0) were titrated to the desired pD by adding different volumes of a 2N NaOH/D_2O solution. 0.2 mg ml^{-1} of NaN_3 were added to all the samples in order to avoid bacterial growth [8]. For basic pD, the ionic strength, I^*, reported in table 1 refers only to the NaOH contribution. The samples were prepared without adding any buffer. The pD value was sequentially checked by an ISFET pH Meter (KS723) before and after each performed experiment. It always resulted in being stable between ±0.1 units in agreement with the reproducibility of the pH meter. All the samples were prepared a few days before the scheduled experiment, in order to allow the H–D exchange. The storing temperature was below 4 °C. In order to be sure that the protein was molecularly dissolved, the high volume fraction samples were prepared from low concentrated solutions by evaporating the solvent using an Ar flux. This is a very tedious but efficient method for sample preparation. The final protein concentration was determined by weight.

Three different salts have been chosen to investigate the anion effect according to the Hofmeister series: NaCl, NaSCN and Na_2SO_4. In the presence of NaCl and NaSCN we examined the anion concentration effect, while Na_2SO_4 has been added only at a concentration 0.33 M in order to compare the sulfate effect with chloride and thiocyanide anions at the same ionic strength (about 1 M). The details of sample compositions are reported in tables 2 and 3.

3. Methods

Neutron scattering measurements were performed at the NG-7 SANS instrument at the NIST Center For Neutron Research (Gaithersburg, MD, USA) using incident monochromatic neutrons of wavelength $\lambda = 5$ Å with $\Delta\lambda/\lambda = 10\%$.

The sample to detector distance was fixed at 2.5 m, covering the magnitude of scattering vector, Q, from 0.0125 to 0.32 Å^{-1}. The detector was a 65 × 65 cm^2 ^{3}He position-sensitive proportional counter having a 5 × 5 mm^2 resolution. The neutron beam size on the sample was

Table 2. The composition of cytochrome C samples at pD = 11.0 in the presence of NaCl and NaSCN at different concentrations.

ϕ (CytC)	[c] (mM)	NaCl (M)	ϕ (CytC)	[c] (mM)	NaSCN (M)
0.010	0.92	0.93	0.010	0.92	0.86
0.100	9.19	0.96	0.099	9.04	0.90
0.208	18.99	0.95	0.211	19.33	0.87
0.299	27.42	0.207	0.301	27.51	0.169
0.301	27.53	0.958	0.299	27.42	0.820
0.300	27.46	1.92	0.299	27.33	1.47
0.300	27.45	2.77	0.299	27.33	2.26
0.349	31.96	0.95	0.347	31.78	0.86
0.401	36.69	0.196	0.397	36.33	0.145
0.400	36.62	0.58	0.399	36.51	0.614
0.402	36.72	0.95	0.400	36.62	1.21
0.400	36.61	1.92	0.396	36.17	1.69
0.445	40.66	0.96	0.447	40.86	0.86
0.496	45.36	0.95	0.496	45.39	0.86

Table 3. The composition of cytochrome C samples at pD = 11.0 in the presence of Na_2SO_4 0.33 M, NaCl 0.96 M and NaSCN 0.90 M.

NaCl		NaSCN		Na_2SO_4	
ϕ (CytC)	[c] (mM)	ϕ (CytC)	[c] (mM)	ϕ (CytC)	[c] (mM)
0.010	0.92	0.010	0.92	0.010	0.92
0.100	9.19	0.099	9.04	0.100	9.15
0.208	18.99	0.211	19.33	0.200	18.33
0.301	27.53	0.299	27.42	0.300	27.50
0.349	31.96	0.347	31.78	0.350	32.02
0.402	36.72	0.400	36.60	0.401	36.66
0.445	40.66	0.447	40.86	0.448	40.96
0.496	45.36	0.496	45.39	0.501	45.78

1.6 cm, being circular in shape. Standard (UV) quartz micro-cylindrical cells having a path length equal to 1 mm were used for the low viscosity samples. The high viscosity samples were contained in titanium demountable cells having two flat quartz windows and being 1 mm in path length. Since the transmission of samples spanned from 90% (for the 0.1 volume fraction of protein) to about 80% (for the 0.5 volume fraction of protein) the multiple-scattering effect was small and was not taken into account.

The measured intensity was corrected for background and empty cell contributions, and for non-uniformities in the detector efficiency by dividing the data, pixel-by-pixel, by the measured scattering from an isotropic scatterer such as plexiglass. The data have been rescaled to the absolute intensity by measuring the beam flux at the sample using a standard polymer sample. The $I(Q)$ versus Q data were obtained by a circular average of the two-dimensional intensity distribution at the detector. The overall data reduction was carried out according to the standard NIST procedures [9]. All the neutron scattering experiments were performed at $T = 20.0 \pm 0.1$ °C and no condensation of water was present on the quartz cell windows. The spectra reported in the following figures have the incoherent background already subtracted out.

Rheological measurements were carried out with a stress-controlled rheometer, Paar Physica Universal Dynamic Spectrometer UDS 200. The experiments were performed with a 'cone-plate' geometry designed for handling small quantities of sample. To limit the amount

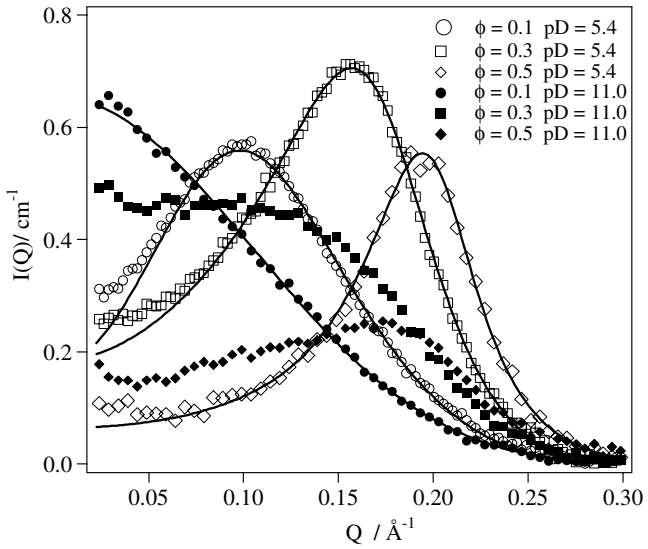

Figure 2. Experimental and fitted scattering intensity distribution as a function of the magnitude of wavevector transfer Q for: $\phi = 0.1$ at pD = 5.4 (experimental data: open circles, ○); $\phi = 0.3$ at pD = 5.4 (experimental data: open squares, □); $\phi = 0.5$ at pD = 5.4 (experimental data: open diamonds, ◇); $\phi = 0.1$ at pD = 11.0 (experimental data: full circles, ●); $\phi = 0.3$ at pD = 11.0 (experimental data: full squares, ■); $\phi = 0.5$ at pD = 11.0 (experimental data: full diamonds, ◆). The solid curve where present represents the fitting results.

of protein needed for the measurement, the cone had a radius 12.5 mm and was placed at 0.05 mm from the plate resulting in a theoretical shear stress range from 0.122 to 36 700 Pa. We performed flow curves varying the shear stress and measuring the shear rate; the viscosity of each point is automatically calculated as the ratio between the preset shear stress and the measured shear rate. All measurements were performed by controlling the shear stress, so that the shear rate range depends on the sample viscosity. All measurements were carried out at a temperature of 20.0 ± 0.1 °C which was regulated by a controlled Peltier system (TEZ 150P) coupled with a Haake circulating bath. The measurements were carried out by imposing shear stress ranges 0.22–2 Pa, 0.2–15 Pa or 0.2–130 Pa according to the sample viscosity.

4. Results and discussions

4.1. pD effect

Figure 2 shows the dependence of the scattering intensity distribution as a function of both protein volume fraction and pD. A pronounced peak, at pD = 5.4, is observed for cytochrome C in the Q range 0.1 and 0.23 Å^{-1} and for volume fractions from 0.1 to 0.5. This broad peak is strictly related to the ordering of protein molecules in solution. In fact, for charged biopolymers there is a minimum of the potential energy at a definite interparticle distance, which is determined by the specific protein volume fraction and charge. The peak shifts to higher Q values with increasing the protein volume fraction and/or the overall charge. Moreover, the width of the SANS peak is the structural evidence of a partial radial order in solution induced by electrostatic interactions between macroions. The analysis of the two-dimensional SANS images did not show any anisotropy even at higher volume fractions and salt addition, in agreement with globally disordered samples. The width of the peak decreases with

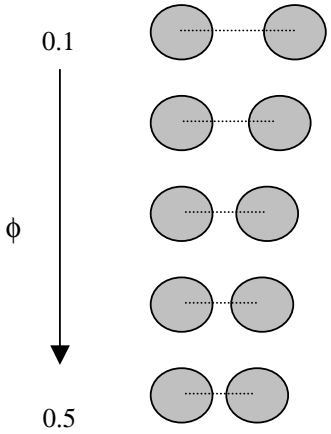

Figure 3. Mean interparticle distance as a function of the volume fraction assuming fcc packing.

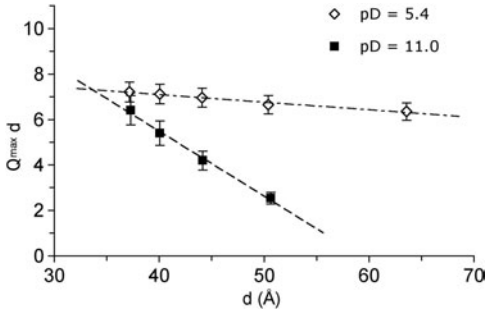

Figure 4. $Q_{\max}d$ as a function of d: pD = 11.0 (full squares, ■) $y = -0.2869x + 16.975$; pD = 5.4 (open diamond, ◇) $y = -0.0334x + 8.4336$.

increasing the biopolymer concentration and the protein charge (see figure 2). At pD = 11.0, the peak maximum shifts at lower Q values, as compared to pD = 5.4 and for the same protein concentration, in agreement with the lower charge expected for a pD closer to the protein isoelectric point. As a general trend, the peak position, $Q_{\max}$, moves to higher Q values when the volume fraction increases at a fixed pD. This can be easily modelled as already done by Chen *et al* [10] in the case of charged micellar solutions. The reported phenomenological approach links the peak position to the mean interparticle distance, d. In order to calculate d, we assumed a face centred cubic (fcc) packing, where all the charged protein molecules are at the same distance from their first neighbours

$$d = \frac{1}{\sqrt{2}}\left(\frac{4000}{N_{\mathrm{A}}[c]}\right)^{1/3} \times 10^7 \text{ Å} \tag{1}$$

where N_{A} is Avogadro's number and $[c]$ is the protein mM concentration as reported in table 1. The interparticle distance is reported in comparison with the cytochrome C dimensions in figure 3. Figure 4 shows the linear trend of $Q_{\max}d$ as a function of d expressed by the equations $Q_{\max}d = 8.434 - 0.0334d$ and $16.98 - 0.2869d$, for pD = 5.4 and 11.0, respectively. These two straight lines cross at about 33 Å, which is consistent with both the protein diameter and the minimum physical interparticle distance (excluding volume contribution), as reported in figure 3. This phenomenological approach is not accurate, since the interaction peaks related to the protein concentrated solutions are not Bragg peaks. The ideal Bragg maxima are shifted to higher Q values mainly due to the negative slope of the form factor (for clarity see figure 5). However, this description qualitatively helps in understanding that the interaction potential is mainly electrostatic and the charge of the protein is strictly linked to the slope of the straight line. At the lowest protein concentration and pD = 11.0 the peak disappears, due to the low charge of the protein, confirming that the broad peak has an electrostatic origin. Summarizing, the increase of cytochrome C concentration and charge promotes a spatial intermolecular ordering in solution. The same trend has already been observed in several charged biopolymers such as proteins and tRNA [11, 12]. Moreover, the three-dimensional Hosemann paracrystalline theory [13] can predict the peak position and broadening if the right order parameter is taken into account [11, 12] proving that the peak is the physical evidence of an interparticle radial order in solution.

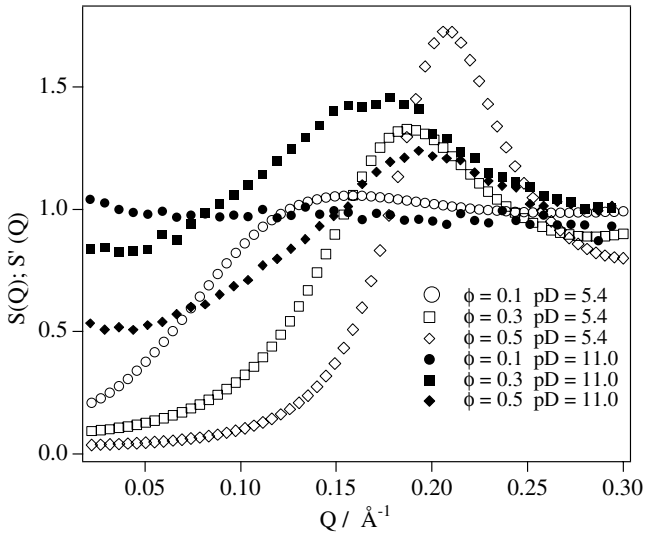

Figure 5. Fitted $S(Q)$ spectra at pD = 5.4, $\phi = 0.1$ (open circles, ○); $\phi = 0.3$ (open squares, □); $\phi = 0.5$ (open diamonds, ◇); 'experimental' $S'(Q)$ curves at pD = 11.0, $\phi = 0.1$ (full circles, ●); $\phi = 0.3$ (full squares, ■); $\phi = 0.5$ (full diamonds, ◆).

The SANS intensity $I(Q)$ of an isotropic solution of protein molecules is described by [8, 14]

$$I(Q) = A_{\mathrm{p}} P(Q) S(Q) + \mathrm{Bkg} \tag{2}$$

where A_{p} is the amplitude factor accounting for the protein number density and the contrast between the scattering object and the solvent, $P(Q)$ is the protein form factor, $S(Q)$ is the protein–protein structure factor and Bkg is the background coming from the incoherent scattering contribution. In the case of cytochrome C, this factor can be written as

$$A_{\mathrm{p}} = [c] \times 10^{-3} N_{\mathrm{A}} [b_{\mathrm{p}a} + N_{\mathrm{ex}}(b_{\mathrm{D}} - b_{\mathrm{H}})\chi + m b_{\mathrm{solv}} - V_{\mathrm{H}} b_{\mathrm{solv}}/v_{\omega}]^2 \tag{3}$$

where N_{A} is Avogadro's number, $[c]$ is the protein concentration in mM, $b_{\mathrm{p}a} = \sum_{\mathrm{p}} b_i = 258.5164 \times 10^{-12}$ cm is the total scattering length of the protein, N_{ex} is the number of labile protons that the protein can exchange with the solvent, b_{H} and b_{D} are the scattering length of the hydrogen and deuterium respectively, m is the number of solvent molecules in the hydration shell, V_{H} is the hydrated protein volume, $v_{\omega} = 30$ Å^3 is the volume of a water molecule, and b_{solv} is the solvent scattering length calculated each time according to the sample composition by using the formula $b_{\mathrm{solv}} = \chi b_{\mathrm{D_2O}} + (1-\chi) b_{\mathrm{H_2O}}$, where χ is the volume fraction of D_2O in the solvent and $b_{\mathrm{D_2O}}$ and $b_{\mathrm{H_2O}}$ are respectively the D_2O and H_2O scattering length. Chen *et al* [8] experimentally determined $N_{\mathrm{ex}} = 165$ and $m = 112$ through contrast variation experiments. $P(Q)$ is the orientational average of the protein form factor, modelled as a core-shell oblate ellipsoid ($a \times b \times b$) having axis ratio $a/b = 0.882\,35$, in agreement with previously published results [8]. In this study we extended the previous analysis by assuming the presence of a constant hydration shell coming from the layers of water molecules bound around the protein surface. The structure factor, $S(Q)$, has been described according to the generalized one-component macroion model (GOCM) already applied to cytochrome C solutions [10]. This model is the extension of the OCM from dilute solutions to finite macroion concentrations.

The parameters that are allowed to change independently are the major core axis b, the shell thickness, the overall protein charge Z, and the background. An amplitude factor has

Table 4. Fitting results using the GOCM model relative to samples at pD = 5.4. SLD = scattering length density.

	pD = 5.4 ± 0.1				
Volume fraction	0.100	0.201	0.300	0.400	0.500
Core major axis (Å)	15.2	15.2	14.4	13.7	13.3
Shell (Å)	1.5	1.3	2.3	2.7	2.2
SLD core ($\times 10^6$) (Å^{-2})	2.906	2.906	2.906	2.906	2.906
SLD shell ($\times 10^6$) (Å^{-2})	5.249	5.161	5.055	4.919	4.743
SLD solvent ($\times 10^6$) (Å^{-2})	6.286	6.160	6.007	5.811	5.557
Charge, Z	4.4	4.7	4.6	4.7	10.5
I^* (M)	—	—	—	—	—
Bkg (cm^{-1})	0.131	0.227	0.268	0.344	0.468

Table 5. Fitting results using the core shell model for an oblate ellipsoid relative to samples at pD = 11.0. SLD = scattering length density.

pD = 11.0 ± 0.1	
Volume fraction	0.093
Core major axis (Å)	12.40
Shell (Å)	5.5
SLD core ($\times 10^6$) (Å^{-2})	2.906
SLD shell ($\times 10^6$) (Å^{-2})	5.250
SLD solvent ($\times 10^6$) (Å^{-2})	6.288
Charge, Z	—
I^* (M)	—
Bkg (cm^{-1})	0.1194

been included to have a further control on the goodness of the fitting. The fitting curves are reported in figure 2 as solid curves, and the corresponding parameters can be found in table 4. In the case of pD = 5.4, the GOCM fits fairly well the experimental data. In particular, a mean value of 16.0 ± 1.5 Å was obtained for the major axis along with a core radius of about 14.0 ± 1.5 Å and a constant protein charge of 4.5 ± 0.2 (table 4). The only exception is at $\phi = 0.5$, where a consistently higher value (10.5) was obtained for the overall protein charge. This discrepancy could also be expected noticing that the peak in this latter case is by far sharper than for the lower volume fractions, $\phi = 0.1$–0.4 (see figure 2). This difference could be ascribed to the presence of an extra term in the interaction potential, meaning that the GOCM model fails to describe very high protein volume fractions, probably because the short-range attractive interaction becomes important when the protein molecules are forced to stay closer. The protein charge can be calculated using the pKa values of the single amino-acid residues reported in table 6 [15] and the pD value. At pD = 5.4 the calculated value of 9.0 is twice the one we found through the fitting procedure (4.5). It should be noticed that, according to the charge renormalization phenomenon [14], the protein charge extracted by the GOCM is the charge experienced by the protein. Its magnitude is due to the ionization of external residues reduced by the counter-ions that adsorb at the interface, and it is usually lower than the calculated one.

In the case of pD = 11.0, the experimental scattering curve relative to $\phi = 0.1$ was fitted using an oblate ellipsoidal core-shell form factor (see the solid curve in figure 2 and table 5) considering the protein–protein interaction negligible, i.e. $S(Q) = 1$. Unfortunately, at this pD, the only form factor approach and the GOCM model fail to describe volume fractions

Table 6. pKa values and abundance number for ionizable residues in horse heart cytochrome C [15].

	N term	Arg	Asp	Glu	His	Lys	Lys	Tyr	C term	Heme A	Heme D
pKa	9.60	14.50	1.00	3.36	6.50	12.40	10.50	10.00	−1.40	2.10	3.00
No a.a.	1	2	3	9	2	11	8	4	1	1	1

higher than 0.1 even taking into account the salt contribution coming from the added NaOH. At this pD, the protein–protein interaction cannot be modelled as a system of oblate ellipsoids interacting by a screened Coulomb potential. The electrostatic nature of the system must be integrated by an attractive part coming from the hydrophobic interactions. Moreover, it should be considered that in a protein molecule the side chains are always charged even if the overall charge can be assumed to be zero (i.e. when the solution has a pD equal to the characteristic pI) so that the formation of ionic couples should also be considered in the attractive contribution. A new theoretical framework is under development to account for the short-range attraction potential, and it will be the subject of a forthcoming paper.

In order to figure out the form of the potential that should be developed, we extracted an 'experimental structure factor', $S'(Q)$, by dividing the scattering intensity distributions at pD $= 11.0$, $I(Q)$, by the form factor, $P(Q)$, extracted from the data at $\phi = 0.1$ and the same pD. These 'experimental structure factors' are shown in figure 5 in comparison with the calculated $S(Q)$ obtained from data at pD $= 5.4$. The peak in the $S(Q)$ moves at higher Q values and its intensity increases as ϕ increases from 0.1 to 0.5. Moreover, $S(Q \rightarrow 0)$ decreases as expected according to the decrease of the osmotic compressibility in a charged colloidal solution with increasing concentration. When the charge of the protein decreases, three main effects are detectable on the structure factor: the shift of the maximum at lower Q, the broadening of the width, and the increase of the osmotic compressibility. All these changes are clear evidence of a decrease in the spatial order induced by the charge as described by the 'paracrystalline' theory [13].

The rheological properties of concentrated cytochrome C solutions were monitored using steady-state viscosity measurements. The rheological behaviour of charged colloidal particles in the case of diluted solutions is characterized by three main electroviscous effects [16]: the interactions of the diffuse double layer around each particle, the balance between electrostatic repulsive force and hydrodynamic compressive force on each particle, and finally the influence of the particle shape. A solution of strongly interacting colloidal particles at high volume fractions and low electrolyte concentrations orders at rest into crystalline lattices as already discussed. If shear is applied, the flow concentrates stress above all at lattice dislocations where particles are loosely trapped. Under flow, the solution's microstructure can be modelled as a 'blend' made up of a solid ordered phase coexisting with a fluid disordered phase, and when the shear rate increases the disordered phase rises above the ordered one. How exactly these phases are organized is still unclear [17]. The rheological behaviour of the solutions we investigated is consistent with this model: the shear leads to a destruction of the ordered structure and the so-called shear-thinning behaviour is observed (i.e. the shear viscosity decreases as the shear rate increases [18]). In this paper we describe only the relative limiting high shear viscosity, $\eta_{rel} = \eta/\eta_0$, as a function of ϕ for both pD. A detailed analysis and modelling of the viscosity curves of the cytochrome C concentrated solutions has been recently reported [18]. As expected, the high shear viscosity exploits a strong concentration dependence increasing with volume fraction, exploiting the maximum value in the case of $\phi = 0.5$ at pD $= 11.0$ (see figure 6).

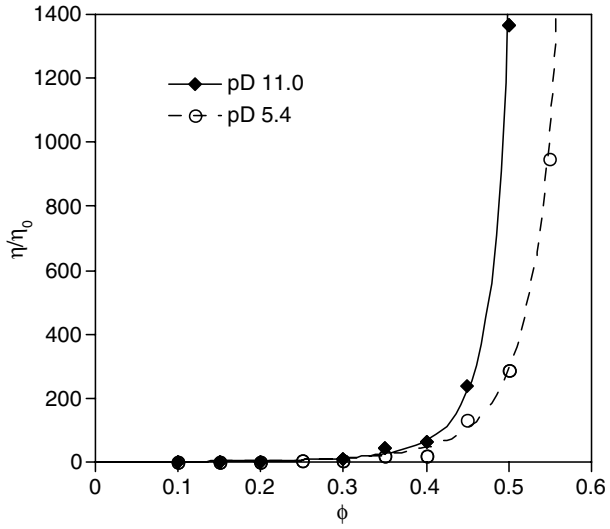

Figure 6. High shear viscosity as a function of cytochrome C volume fraction: pD = 11.0 (experimental data: full diamonds, ♦; fitted curve: solid curve), pD = 5.4 (experimental data: open circles, ○; fitted curve: dashed curve).

Table 7. Fitting parameters ($[\eta]$, ϕ_{max}) using the Krieger–Dougherty equation relative to the protein samples at pD = 5.4 and 11.0 considering an intermediate shear rate (100 s^{-1}) and the infinite shear rate limit.

	Shear rate 100 s^{-1}		Infinite shear rate limit	
pD	ϕ_{max}	$[\eta]$	ϕ_{max}	$[\eta]$
5.4 ± 0.1	0.566 ± 0.064	4.6 ± 0.8	0.584 ± 0.025	5.0 ± 0.4
11.0 ± 0.1	0.574 ± 0.020	6.2 ± 0.5	0.564 ± 0.005	5.9 ± 0.1

Generally, in charged systems the viscosity increases with the effective surface charge [19], but this is not our case. At pD = 5.4, cytochrome C molecules have a greater positive charge (9.0 considering the pKas [15] and 4.5 from the fitting) and consequently experience higher electrostatic repulsions with respect to pD = 11.0 where the overall charge is almost zero (−4.1 considering the pKas and is not detectable by the fitting at $\phi = 0.1$), but shear viscosities relative to pD = 11.0 are higher than those at pD = 5.4.

This means that other effects contribute to the rheological behaviour of the investigated systems, i.e. the aggregation phenomenon is favoured at pD = 11.0 due to the attractive surface of the low charged protein; moreover, this effect enhances with concentration.

The viscosity data can be fitted using the well-known Kieger–Dougherty relation [20]:

$$\eta_{rel} = \frac{\eta}{\eta_0} = \left(1 - \frac{\phi}{\phi_{max}}\right)^{-[\eta]\phi_{max}} \tag{4}$$

where the parameters to be fitted, $[\eta]$ and ϕ_{max}, are the intrinsic viscosity and the volume fraction corresponding to the maximum packing respectively, while η_0 is the solvent viscosity. Table 7 reports $[\eta]$ and ϕ_{max} at the limiting shear rate and 100 s^{-1}. The maximum packing fraction and the intrinsic viscosity appear to be almost shear rate independent: on increasing the shear rate the particle packing is already defined by the repulsive or attractive interaction. At lower shear rates the model is not applicable, since all the viscosity curves collapse.

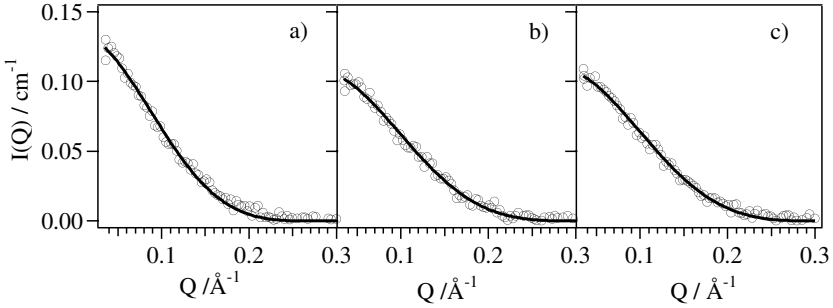

Figure 7. Experimental (open circles, ○) and fitted (solid curve) SANS spectra relative to solutions with $\phi = 0.01$ and: (a) 1.0 M NaCl; (b) 1.0 M NaSCN; (c) 0.33 M Na_2SO_4.

The behaviour of protein solutions changes from liquid-like to solid-like as the volume fraction approaches maximum packing. Different values have been reported in the literature for suspensions of monodisperse particles. These results indicate that the maximum packing fraction may change significantly with purity, shape, relative monodispersity of the particles, and the level of accuracy of experiments. As a reference it is worth reporting that a system constituted of perfect spheres has an intrinsic viscosity value equal to 2.5, and this value strongly depends on the shape and surface roughness of the particles [21]. In particular, deviations from spherical symmetry cause an increase in the $[\eta]$ magnitude that usually ranges from 2.5 (spheres) to 10 (plates). Additionally, the aggregation (polydispersity) may also be responsible for the high intrinsic viscosity. So the obtained values of 5.0 and 5.9, for pD = 5.4 and 11.0, respectively, are a reasonable consequence of the ellipsoidal native shape of cytochrome C mixed with the high complexity of the investigated solutions that involves some sort of aggregation to give more asymmetric and polydisperse structures. A higher value is found in the case of higher pD, confirming that the aggregation is favoured by the low surface charge. The system at pD = 11.0 is characterized by higher ϕ_{max} values. In particular, electrostatic interactions become less effective while the shear rate increases. We can conclude that in the high shear rate region excluded volume effects are more effective than electrostatic ones in affecting the maximum packing values.

4.2. Salt effect

The salt effect investigation was performed at pD = 11.0 to check the protein–anion specific interaction. In fact, at this pD the protein is weakly negatively charged and the anion cannot interact simply via an electrostatic attraction as in the case of low pD. The polarizability term of the interaction should be enhanced and the Hofmeister effect would be dominant.

In order to verify that the protein does not change in shape upon the addition of salt, we investigated SANS spectra at very low protein volume fraction, $\phi = 0.01$. As shown in figure 7, the spectra were fitted using a core-shell oblate ellipsoid, with the axial ratio fixed to 0.882 35. The parameters describing $P(Q)$ are reported in table 8.

Useful information on the shape and compactness of the protein in solution can be extracted by using the Kratky representation, usually applied to clarify the folding state in a protein (see for example [22]). In the Kratky plot [23] the scattering intensity multiplied by the square of the scattering wavevector is plotted against the scattering wavevector (see figure 8). The scattering profile relative to biopolymers in a random coil state falls off as $1/Q$ due to the randomly oriented segments of the polypeptide chain whose scattering cancels out. Hence, in

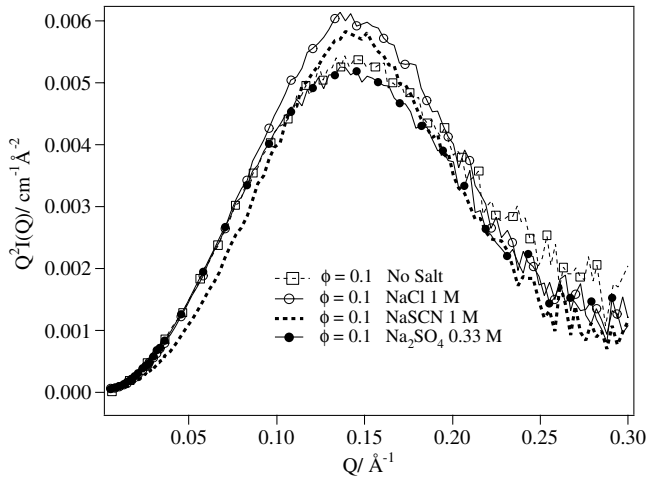

Figure 8. Kratky plots for cytochrome C solutions at: $\phi = 0.1$ and no salt (dashed curve, open squares, □); 1.0 NaCl (solid curve, open circles, ○); 1.0 M NaSCN (dotted curve); 0.33 M Na_2SO_4 (solid curve, full circle, ●).

Table 8. Fitting results using the form factor for an oblate ellipsoid relative to the curves in figure 7. $\Delta\rho$ = contrast.

	NaSCN	Na_2SO_4	NaCl
Volume fraction	0.01	0.01	0.01
Core major axis (Å)	14.2	14.1	15.2
Shell (Å)	4.8	5.3	6.4
$\Delta\rho_{\text{core-shell}}$ ($\times 10^6$) (Å^{-2})	−2.407	−2.407	−2.407
$\Delta\rho_{\text{shell-solvent}}$ ($\times 10^6$) (Å^{-2})	−1.066	−1.066	−1.066
Bkg (cm^{-1})	0.069	0.068	0.069

the Kratky plot, at high Q values the scattering trend is proportional to the scattering vector. On the other hand, as shown by Porod [23], the surface of a compact protein produces a scattering profile proportional to $1/Q^4$, which in a $Q^2I(Q)$ representation reduces to a $1/Q^2$ trend. Consequently, the Kratky plot is helpful in determining the protein state, as the native or molten globule conformations show a pronounced peak, while the fully denatured states show a characteristic upward rising feature [22]. This treatment is based on the assumption that the scattered intensity is a pure form factor and is applicable only in the low ϕ cases. As we can see from figure 8, the addition of different salts does not have a dramatic effect on the shape of the protein, leaving its conformation very compact and the cytochrome C globular.

As a first guess, the radius of gyration (R_g) has been experimentally determined from the scattering spectra using the Guinier plot [23] $\ln I(Q)$ versus Q^2, with the Guinier approximation $I(Q) = 1 - Q^2R_g^2/3$. In the case of cytochrome C, it is well-accepted that R_g increases from 14 Å for the native state at pH 7 to 24.2 and 32.4 Å for the unfolded state in the case of pH = 2 without and with the addition of guanidium hydrochloride, passing through 17.4 Å for the molten globule state obtained at pH = 2 with 0.4 M of NaCl [24]. The Guinier plots of the spectra reported in figure 7 have a linear region from 0.002 up to 0.012 Å^{-2}. The R_g values are obtained by the linear fit of this region up to 0.008 Å^{-2}, the highest Q satisfying an empirical criterion for Guinier fit, $QR_g < 1.3$, according to the literature [25]. The values

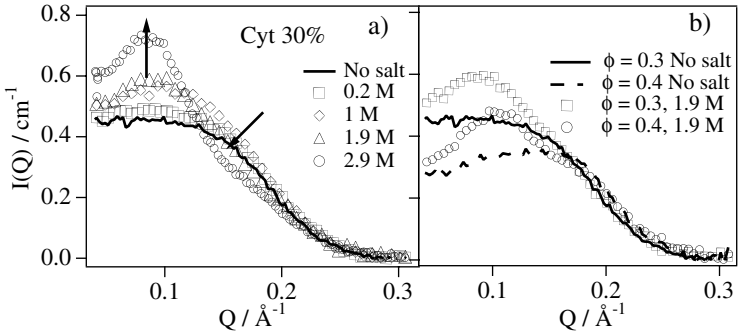

Figure 9. (a) Experimental SANS spectra relative to cytochrome C solutions as a function of NaCl concentration at ϕ 0.3; (b) comparison of scattering intensity distributions at ϕ 0.3 and 0.4 with [NaCl] = 1.9 M.

found for the different salts are: 13.5 ± 0.7, 11.2 ± 0.6 and 11.0 ± 0.6 Å for chloride, sulfate and thiocyanate anions. The theoretical charge values calculated from the pKas are 19.4, 7.5 and -4.1 for pH = 2.0, 7.0 and 11.0, respectively. A lower value of R_g with respect to the native state can be ascribed to two factors. In our case the protein has a lower charge with respect to the neutral pH case, resulting in a more compact structure than in the native case. In addition, the salts screen the residual charge, enhancing the compactness of the globule. This effect is maximum for sulfate and thiocyanate that are at the opposite sides in the Hofmeister series, while the chloride anion is close to water in the HS. A large excess of the three investigated salts does not denature the protein, keeping its shape globular and increasing its compactness. These results are in agreement with the more appropriate ellipsoidal model reported above (see figure 7 and table 8).

Figure 9(a) illustrates the effect of increasing sodium chloride concentration for volume fractions of protein equal to 0.3. At low salt concentration (0.2 M), the effect of the salt is negligible. Additional salt has the effect of shifting the interaction peak to lower Q values. In particular the peak shifts from 0.14 to 0.085 and 0.095 $Å^{-1}$ in the case of volume fraction 0.3 and 0.4, respectively (see figure 9(b)). The associated interparticle dimensions ($d = 2\pi/Q_{max}$) are 74–66 Å, i.e. about twice the cytochrome C diameter. Ion association favours the formation of multimers (dimer, tetramer or octamer), and an equilibrium between multiple species cannot be excluded.

At the same volume fractions NaSCN produces stronger effects than NaCl on the scattering intensity distribution as reported in figure 10. Again, low salt concentration has negligible effect. The appealing feature is that a very strong interaction peak develops for Q below 0.05 $Å^{-1}$. Again, the lower the volume fraction the higher the peak position: for $\phi = 0.4$ and 0.30 the peak position is at 0.045 and 0.035 $Å^{-1}$, respectively (see figure 10(b)). The associated dimensions 209–125 Å agree with very large clusters (4–7 times the protein diameter). Hence if the peak position is related to the cluster dimension the thiocyanate anion induces bigger aggregates than chloride. Moreover, even if the new peak with NaSCN is sharper than with NaCl the 2D SANS images did not evidence any anisotropy.

Recently, Sciortino *et al* [26] evidenced that in colloidal systems and in protein solutions, governed by both a short range attractive interaction and a weak electrostatic repulsion, the appearance of a low Q peak can be related to the formation of clusters in equilibrium with single particles. A gel phase can appear stabilized, differently to the common view of the short-range attraction, by the presence of a weak long-range screened electrostatic repulsive interaction.

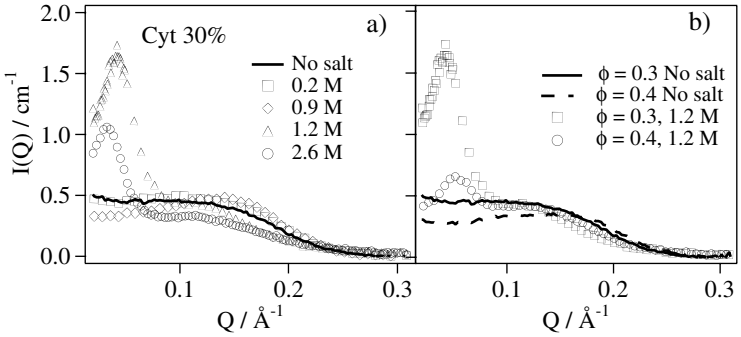

Figure 10. (a) Experimental SANS spectra relative to cytochrome C solutions as a function of NaSCN concentration at ϕ 0.3; (b) comparison of scattering intensity distributions at ϕ 0.3 and 0.4 with [NaSCN] = 1.2 M.

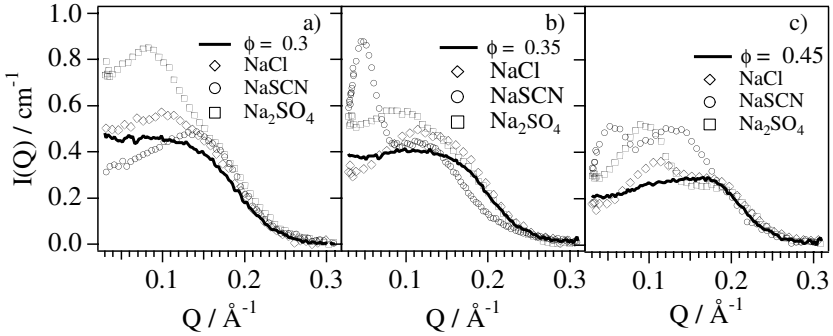

Figure 11. Experimental SANS spectra relative to cytochrome C solutions. (a) $\phi = 0.3$ and: no salt (solid curve); 0.96 M NaCl (open diamonds, ◇, solid curve); 0.86 M NaSCN (open circles, ○); 0.33 M Na_2SO_4 (open squares, □, solid curve); (b) $\phi = 0.35$ and no salt (solid curve); $\phi = 0.5$ (dotted curve); $\phi = 0.45$: 0.96 M NaCl (open diamonds, ◇, solid curve); 0.86 M NaSCN (open circles, ○); 0.33 M Na_2SO_4 (open squares, □, solid curve); (c) $\phi = 0.45$ and no salt (solid curve); 0.96 M NaCl (open diamonds, ◇, solid curve); 0.86 M NaSCN (open circles, ○); 0.33 M Na_2SO_4 (open squares, □, solid curve).

The two peaks in the spectra can be interpreted as the cluster–cluster interaction concurrent to the protein–protein interaction. Eventually, the increase of the cluster concentration can dynamically quench the structure by the glass transition phenomenon [2].

Figure 11(a) shows the SANS spectra for cytochrome C at $\phi = 0.3$ in the presence of sulfate, thiocyanate and chloride at a fixed ionic strength of about 1 M referred to the case without added salt. The interesting feature is the peak position in the spectra with SO_4^{2-} and Cl^-. Here the maximum falls at lower Q values than SCN^- and without added salt. In particular, the position of the peaks increases from $SO_4^{2-} < Cl^- < SCN^-$, indicating that the cluster dimensions decrease in the same order. Besides, with SO_4^{2-} and Cl^- there is a shoulder at Q values corresponding to the protein–protein interaction peak (the maximum for no added salt and SCN^-). The peak shift at low Q for these two anions is due to a cluster–cluster interaction in addition to the macroion–macroion interaction.

When the protein volume fraction is increased to $\phi = 0.35$ the SANS spectra relative to solutions in the presence of thiocyanate change, and a second interaction peak at about 0.05 $Å^{-1}$ appears (see figure 11(b)), the salt/protein molar ratio, 27.5, resulting in being optimum for

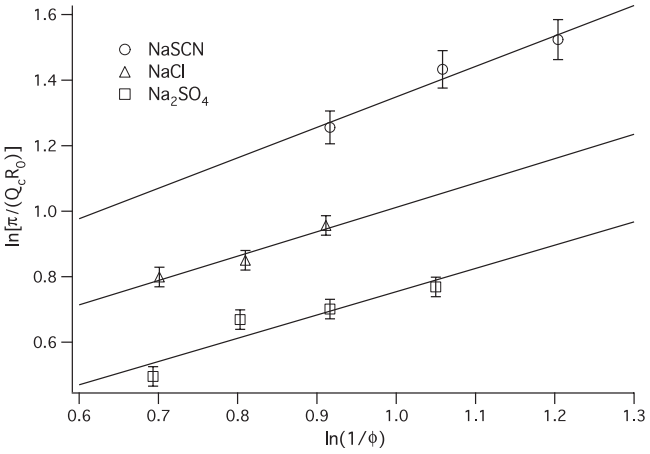

Figure 12. Plots of $\ln(\pi/Q_c/R_0)$ as a function of $\ln(1/\phi)$ for NaSCN, NaCl and Na_2SO_4. The data have been offset for clarity reasons.

cluster formation. Instead, SO_4^{2-} and Cl^- do not produce any change in the shape of the spectra, except that the protein–protein interaction peak becomes more evident.

On increasing ϕ up to 0.45, sulfate and chloride ions also become effective in inducing cluster formation, and the two peaks separate (see figure 11(c)). At this protein concentration the anion/protein molar ratio is about 21, 24 and 8 for SCN^-, Cl^- and SO_4^{2-} respectively. It must be observed that, on increasing the protein volume fraction and decreasing the salt/protein molar ratio, the scattering intensity decreases consistently in all the investigated Q range. Considering the case without salt added, the low Q peak is not present even at $\phi = 0.5$, as reported in figure 2.

The occurrence of a cluster peak has already been observed by Giglio and co-workers in the case of a simple colloidal system [27, 28]. They studied polystyrene solutions and added $MgCl_2$ to induce aggregation. Monitoring the light scattering intensity distribution as a function of time, they found a finite Q peak given by the aggregate formation. The peak intensity and position developed in time up to the so-called terminal time-independent state. This latter state is what we observe in the reported SANS spectra of cytochrome C. Considering the terminal gel state as consisting of a system of space-filling ordered fractal clusters of proteins of dimension d_f, the average cluster size, R_{max}, can be related to the volume fraction ϕ of the proteins, by means of the following relation [27, 28]:

$$\left(\frac{R_{max}}{R_0}\right)^{d_f-3} = \left(\frac{4\pi c_0 R_0^3}{3}\right) = \phi \tag{5}$$

where c_0 is the number density of the protein and R_0 its radius (16.3 Å).

We now consider the low Q peak in the SANS intensity distribution to arise from these ordered fractal clusters; then we can estimate the cluster–cluster correlation peak position to occur at $Q_c = \alpha\pi/R_{max}$, where α is a constant of order unity, and equation (5) can be recast into the form

$$\ln\left(\frac{\pi}{Q_c R_0}\right) = \ln\left(\frac{1}{\alpha}\right) + \frac{1}{3-d_f}\ln\left(\frac{1}{\phi}\right) \tag{6}$$

where Q_c is the cluster–cluster interaction peak position.

Figure 12 shows the straight lines that best describe $\ln(\pi/Q_c R_0)$ as a function of $\ln(1/\phi)$ for the series of investigated samples spanning different protein volume fractions and the same salt concentration. Different slopes indicate different fractal dimensions. In particular, d_f is 1.92, 1.65 and 1.59 for SCN^-, Cl^- and SO_4^{2-}, respectively, and therefore clusters become less

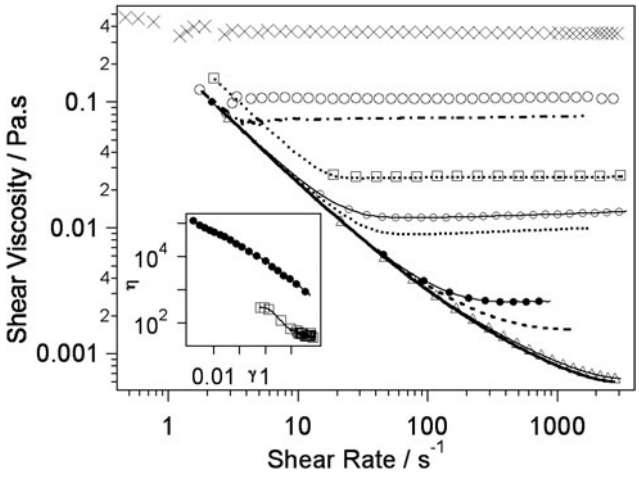

Figure 13. Experimental shear viscosity is reported as a function of shear rate for samples at pD = 11.0: $\phi = 0.1$ (solid curve); $\phi = 0.1$, NaCl 0.95 M (solid curve, open triangle, △); $\phi = 0.2$ (dashed curve); $\phi = 0.2$, NaCl 0.95 M (solid curve, full circles, ●); $\phi = 0.3$ (dotted curve); $\phi = 0.3$, NaCl 0.21 M (solid curve, open circles, ○); $\phi = 0.3$, NaCl 2.8 M (dotted curve, open squares, □); $\phi = 0.4$ (dash–dotted curve); $\phi = 0.4$, NaCl 0.6 M (open circles, ○); $\phi = 0.4$, NaCl 1.9 M (crosses, ×). Inset: $\phi = 0.45$, NaCl 0.96 M (solid curve, open squares, □); $\phi = 0.5$, NaCl 0.96 M (full circles, ●).

dense passing from thiocyanate to sulfate. The value for SCN^- resembles an RLCA kinetic, while the values for Cl^- and SO_4^{2-} are lower than the universal pure DLCA, 1.81. The low Q peak position is shifted towards higher Q values with sulfate and chloride, meaning that these anions favour smaller and more tenuous clusters. This is in agreement with rheological data showing a higher viscosity increase with SCN^- (see later in the text). The d_f trend resembles the Hofmeister series where Cl^- represents a borderline case, and sulfate and thiocyanate are at the opposite side, sulfate being a so-called kosmotropic ion and thiocyanate a chaotropic ion. In particular d_f increases in the order: $SO_4^{2-} < Cl^- < SCN^-$.

In order to have a deeper insight on the effect of salt addition on the dynamical properties of the cytochrome C concentrated solutions we carried out viscosity measurements. In figures 13–15 the viscosities are given as a function of shear rate for samples at different protein volume fractions in the presence of NaCl, NaSCN and Na_2SO_4, respectively. In the case of NaCl and NaSCN we also report, in figure 16, the trends of the relative high shear viscosity as a function of salt concentration.

In presence of NaCl the flow behaviour remains unchanged at lower protein volume fractions: shear thinning is observed up to volume fraction 0.3, while at $\phi = 0.4$ the samples present a Newtonian behaviour in the accessible shear rate range (see figure 13). From figure 15, it is clear that the addition of NaCl up to 1 M to the protein with $\phi = 0.1$ has no effect on the shear viscosity. At higher volume fractions (from 0.2 to 0.4) the addition of chloride increases the high shear viscosity plateau values. The inset of figure 13 shows the trend of the shear viscosity as a function of the shear rate relative to cytochrome C solutions for two protein volume fractions, 0.45 and 0.5, and 0.96 M NaCl concentration. The presence of salt changes the flow curves; in particular at $\phi = 0.45$, a shear thinning behaviour with a low shear plateau and a high shear plateau can be recognized, while at $\phi = 0.5$ the high shear viscosity plateau is not reached within the experimental stress range (i.e. 36 700 Pa).

The salt effect on the viscosity strongly depends on the protein volume fraction: a 2.8 M NaCl concentration at $\phi = 0.3$ produces a 1.6% relative increase in the shear viscosity, while

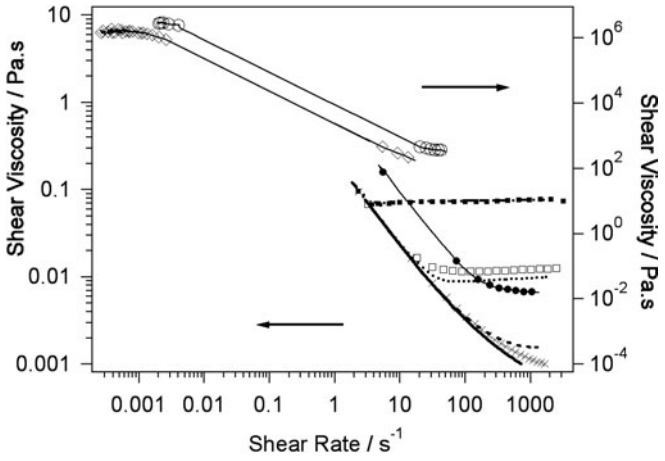

Figure 14. Experimental shear viscosity is reported as a function of shear rate for samples at pD = 11.0: $\phi = 0.1$ (solid line); $\phi = 0.1$ and NaSCN 0.86 M (crosses, ×); $\phi = 0.2$ (dashed line); $\phi = 0.2$ and NaSCN 0.86 M (solid line, full circles, ●); $\phi = 0.3$ (dotted line); $\phi = 0.3$ and NaSCN 0.17 M (open squares, □); $\phi = 0.3$ and NaSCN 2.3 M (solid line, open diamonds, ◇); $\phi = 0.4$ (dash–dotted line); $\phi = 0.4$ and NaSCN 0.15 M (full squares, ■); $\phi = 0.4$ and NaSCN 1.7 M (solid line, open circles, ○).

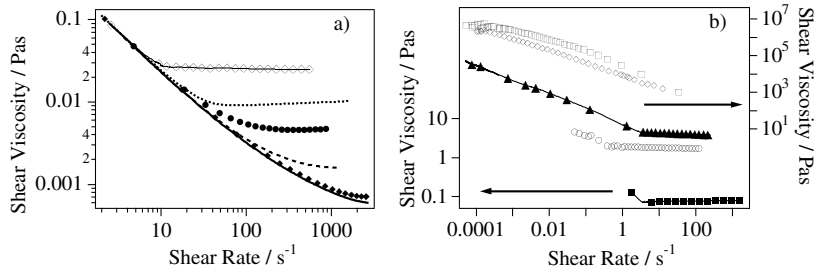

Figure 15. Experimental shear viscosity is reported as a function of shear rate for samples at pD = 11.0 and 0.33 M Na_2SO_4: (a) $\phi = 0.1$ (full diamonds, ♦), $\phi = 0.2$ (full circles, ●), $\phi = 0.3$ (solid curve, open diamonds, ◇); (b) $\phi = 0.4$ (solid line, full triangles, ▲), $\phi = 0.45$ (open diamonds, ◇), $\phi = 0.5$ (open squares, □). For comparison we also reported the curves without salt: (a) $\phi = 0.1$ (solid curve); $\phi = 0.2$ (dashed curve); $\phi = 0.3$ (dotted curve); (b) $\phi = 0.4$ (solid curve, full squares, ■); $\phi = 0.50$ (open circles, ○).

a lower NaCl concentration, 1.9 M at $\phi = 0.4$, causes a higher relative increase (i.e. 3.7%) (see figure 13). At $\phi = 0.5$ the increase is even more remarkable (i.e. 380%), the viscosity increasing from 1.78 Pa s without salt to 679 Pa s with 0.96 M NaCl (see inset of figure 13). It is important to stress that the higher the protein volume fraction the lower the effective NaCl concentration per unit of macroion.

The NaSCN addition produces a noticable increase of the high shear viscosity plateau value already at a volume fraction 0.1 (figure 14). At concentrations lower than 1.5 M the flow behaviour is retained, but a low shear Newtonian plateau can be detected at NaSCN concentrations higher than 1.5 M at both cytochrome C volume fractions 0.3 and 0.4, and an increase of shear viscosity of about three magnitude orders is observed (see figure 14). The limiting value obtained after the structural arrest is the same for different protein volume fractions.

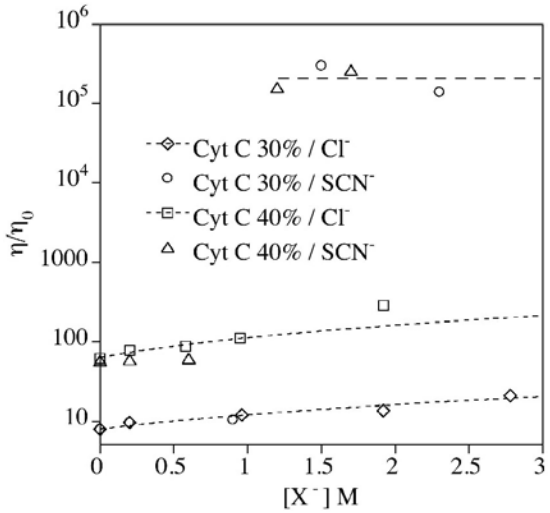

Figure 16. High shear viscosity as a function of NaCl and NaSCN concentration at cytochrome C volume fraction $\phi = 0.3$ and NaSCN (open circles, ○); $\phi = 0.3$ and NaCl (open diamonds, ◇); $\phi = 0.4$ and NaSCN (open triangles, △); $\phi = 0.4$ and NaCl (open squares, □). The dashed lines are only a guide for the eye.

Figure 15 reports the profiles of the shear viscosity as a function of the shear rate for protein samples with increasing volume fraction and in the presence of 0.33 M Na_2SO_4. Curves relative to samples from $\phi = 0.1$ to 0.4 present a shear thinning behaviour with a high shear rate viscosity plateau. The viscosity enormously increases when the protein volume fraction reaches 0.45: from about 5.5 Pa s at $\phi = 0.4$ to about 1500–2000 Pa s at $\phi = 0.45$ and 0.5. For these two last samples the high shear viscosity plateau was not experimentally accessible since fracture in the sample is induced by the high shear stress, 19 600 and 34 600 Pa in the case of 0.45 and 0.5, respectively. This phenomenon was also observed in some heat-denatured whey protein gels at high ionic strength where the so-called particulate gel was formed, and a relation was found between the fracture strain and the floc dimensions. In particular, particulate gels formed at high ionic strength become more brittle with decreasing floc dimensions [29]. This is in agreement with the lower fractal dimensions of cytochrome C gels with sulfate anions.

As with thiocyanate and chloride, the sulfate anion produces an increase of the high shear viscosity and its effect depends on protein concentration.

The first evidence of the salt addition is the rise of the limiting high shear viscosity that confirms that the aggregation phenomenon is taking place in solution. We have already mentioned the competition between electrostatic and aggregation phenomena in determining the high shear plateau values and shown that the last one is dominant. At pD = 11.0 and in the presence of salt adsorbing at protein surface, the salt makes the aggregation process more favourable, inducing a shear viscosity rise; the more effective the anion adsorption the larger the shear viscosity increase.

With Cl^- and SCN^- we evaluated the effects on high shear viscosity as a function of salt concentration in figure 16. It is evident that NaCl has very little effect on the high shear viscosity if compared with NaSCN, suggesting an 'anion specificity'.

The samples with NaCl show a linear trend of the relative viscosity as a function of salt concentration, and the slopes of the curves are dependent on protein concentration: 4 at $\phi = 0.3$ and 50 at $\phi = 0.4$ (the last sample at [Cl^-] 1.9 M deviates from the linear trend).

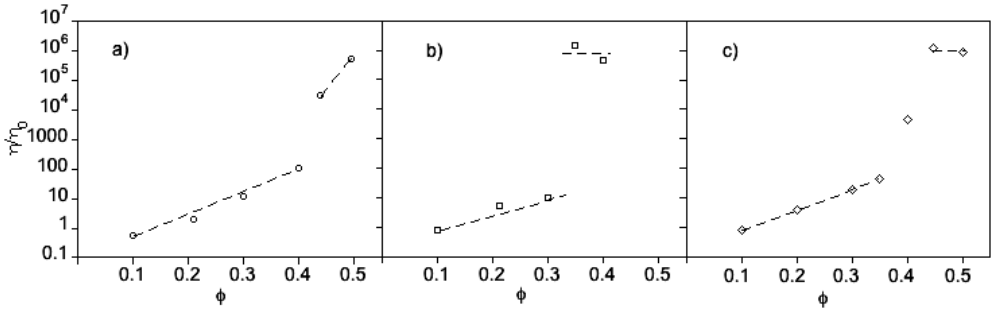

Figure 17. High shear viscosity as a function of cytochrome C volume fraction at pD = 11.0 with anions: (a) chloride; (b) thiocyanate; (c) sulfate. The dashed lines are only a guide for the eye.

With NaSCN (see figure 16) we can recognize a threshold in the salt concentration with a jump in viscosity values for a concentration c^*. This threshold concentration depends slightly on the protein volume fraction. In fact, at $\phi = 0.3$ the threshold occurs between 1.0 and 1.5 M; on increasing the protein volume fraction, c^* exhibits lower values: $0.6\,\mathrm{M} < c^* < 1.2\,\mathrm{M}$. The value of c^* can be considered as the concentration of salt that produces the structural arrest in the protein sample. At concentrations below this threshold a linear dependence of the relative viscosity as a function of NaSCN concentration is found for both 0.3 and 0.4 protein volume fractions.

Figure 17 reports the relative limiting high shear viscosity, $\eta_{\mathrm{rel}} = \eta/\eta_0$, as a function of ϕ for the three studied anions. With Cl^- between $\phi = 0.4$ and 0.45 the relative viscosity grows by three orders of magnitude; with SCN^-, from $\phi = 0.3$ to 0.35 the relative viscosity increase is even higher, i.e. four orders of magnitude, and with SO_4^{2-}, in the ϕ range between 0.35 and 0.45, a four orders of magnitude rise in the relative viscosity can be recognized with an intermediate situation at ϕ 0.4. The anion nature controls both the threshold value and the extent of relative viscosity growth.

5. Conclusions

In protein solutions of cytochrome C SANS intensity distributions at pD = 5.4 (positively charged) show an interaction peak which shifts to larger Q with increasing volume fraction. SANS spectra can be fitted with the protein–protein potential (PMF) which is a screened Coulomb (one-Yukawa) form with the protein charge of about 5 units. The high shear viscosity diverges at a characteristic volume fraction of 0.58, and the intrinsic viscosity has a value of 5.0.

SANS intensity distributions at pD = 11.0 (slightly negatively charged) show a broad shoulder which shifts to larger Q on increasing the protein volume fraction. They, however, cannot be fitted with a PMF of one-Yukawa form, suggesting the presence of protein–protein attractive interactions in addition. The low shear viscosity diverges at a characteristic volume fraction of 0.56, which is lower than that of the pD = 5.4 (repulsive) case, and the intrinsic viscosity has a value of 5.9.

The addition of different monovalent co-ions at pD = 11.0 triggers the growth of attractive interaction which gives rise to an additional low Q peak in the SANS intensity distribution. The low Q peak height is dependent on the amount of added salt and on the kind of co-ion. Interestingly, the ability of a given co-ion to induce the attraction follows a Hofmeister series. The appearance of a low Q peak in the small angle neutron scattering spectra is also

accompanied by a strong increase in the relative viscosity. These phenomena taken together can be considered as the signature of the gelation process promoted by specific co-ion interactions.

Acknowledgments

The authors express their thanks to C J Glinka (NCNR, Gaithersburg) for help with the experimental setup and to the NIST Center For Neutron Research (NCNR, Gaithersburg) for allocating neutron beam time at the NG7-SANS spectrometer. The research of SHC is supported by a grant from the Materials Research Program of the US DOE. Finally, BL, EF and PB acknowledge MIUR (PRIN-2003 grant) and the Consorzio Interuniversitario per lo Sviluppo dei Sistemi a Grande Interfase (CSGI, Florence, Italy) for partial financial support.

References

[1] McPherson A 1999 *Crystallization of Biological Macromolecules* (New York: Cold Spring Harbor Laboratory Press)
[2] Goetze W 1991 *Liquids, Freezing and Glass Transition* ed J P Hansen, D Levesque and J Zinn-Justin (Amsterdam: North-Holland) p 287
[3] Hofmeister F 1888 *Arch. Exp. Pathol. Pharmakol. (Leipzig)* **24** 247
[4] Eagland D 1975 *Water a Comprehensive Treatise* ed F Franks (New York: Plenum) p 305
[5] Collins K D and Washabaugh M W 1985 *Q. Rev. Biophys.* **18** 323
[6] Carbonnaux C, Ries-Kautt M and Ducruix A 1995 *Protein Sci.* **4** 2123
[7] Ries-Kautt M and Ducruix A 1989 *J. Biol. Chem.* **264** 745
[8] Wu C-F and Chen S-H 1987 *J. Chem. Phys.* **87** 6199
[9] http://www.ncnr.nist.gov/programs/sans/manuals/data_red.html
[10] Chen S-H and Sheu E Y 1990 *Micellar Solutions and Microemulsions* ed S-H Chen and R Rajagopalan (Berlin: Springer)
[11] Matsuoka H, Ise N, Okubo T, Kunugi S, Tomiyama H and Yoshikawa Y 1985 *J. Chem. Phys.* **83** 378
[12] Häußler W, Wilk A, Gapinski J and Patkowski A 2002 *J. Chem. Phys.* **117** 413
[13] Hosemann R and Bagchi S N 1962 *Direct Analysis of Diffraction by Matter* (Amsterdam: North-Holland)
[14] Wu C-F and Chen S-H 1988 *Biopolymers* **27** 1065
[15] Zhou H-X and Vijayakumar M 1997 *J. Mol. Biol.* **267** 1002
[16] Russel W B 1979 *J. Fluid Mech.* **92** 401
[17] van der Vorst B, van den Ende D, Aelmans N J J and Mellema J 1997 *Phys. Rev.* E **56** 3119
[18] Lonetti B, Fratini E, Chen S H and Baglioni P 2004 *Phys. Chem. Chem. Phys.* **6** 1388
[19] Horn F M and Richtering W 2000 *J. Rheol.* **44** 1279
[20] Goodwin J W and Hughes R W 2000 *Rheology for Chemists–An Introduction* (Cambridge: The Royal Society of Chemistry)
[21] Barnes H A 1999 *J. Non-Newton. Fluid. Mech.* **81** 133
[22] Doniach S 2001 *Chem. Rev.* **101** 1763
[23] Glatter O and Kratky O 1982 *Small Angle X-ray Scattering* (New York: Academic)
[24] Hamada D, Kuroda Y, Kataoka M, Aimoto S, Yoshimura T and Goto Y 1996 *J. Mol. Biol.* **256** 172
[25] Hamada D, Hoshino M, Kataoka M, Fink A L and Goto Y 1993 *Biochemistry* **32** 10351
[26] Sciortino F, Mossa S, Zaccarelli E and Tartaglia P 2003 *Preprint* cond-mat/0312161
[27] Carpineti M and Giglio M 1993 *Phys. Rev. Lett.* **70** 3828
[28] Carpineti M and Giglio M 1993 *Phys. Rev. Lett.* **71** 656
[29] Ikeda S, Foegeding E A and Hagiwara T 1999 *Langmuir* **15** 8584